



# Ultrafast excited-state dynamics of Luteins in the major light-harvesting complex LHCII

Laura Pedraza-González<sup>1</sup> · Davide Accomasso<sup>1</sup> · Lorenzo Cupellini<sup>1</sup> · Giovanni Granucci<sup>1</sup> · Benedetta Mennucci<sup>1</sup>

Received: 5 October 2023 / Accepted: 23 November 2023 / Published online: 27 December 2023  
© The Author(s) 2023

## Abstract

Carotenoid pigments are known to present a functional versatility when bound to light-harvesting complexes. This versatility originates from a strong correlation between a complex electronic structure and a flexible geometry that is easily tunable by the surrounding protein environment. Here, we investigated how the different L1 and L2 sites of the major trimeric light-harvesting complex (LHCII) of green plants tune the electronic structure of the two embedded luteins, and how this reflects on their ultrafast dynamics upon excitation. By combining molecular dynamics and quantum mechanics/molecular mechanics calculations, we found that the two luteins feature a different conformation around the second dihedral angle in the luminal side. The *s*-cis preference of the lutein in site L2 allows for a more planar geometry of the  $\pi$ -conjugated backbone, which results in an increased degree of delocalization and a reduced excitation energy, explaining the experimentally observed red shift. Despite these remarkable differences, according to surface hopping simulations the two luteins present analogous ultrafast dynamics upon excitation: the bright  $S_2$  state quickly decays (in  $\sim 50$  fs) to the dark intermediate  $S_x$ , eventually ending up in the  $S_1$  state. Furthermore, by employing two different theoretical approaches (i.e., Förster theory and an excitonic version of surface hopping), we investigated the experimentally debated energy transfer between the two luteins. With both approaches, no evident energy transfer was observed in the ultrafast timescale.

## Graphical abstract

## 1 Introduction

Carotenoid pigments (Cars) exhibit a versatile role in both light-harvesting and photoprotection functions when they are bound to light-harvesting complexes (LHCs) [1–7]. Numerous experimental and theoretical studies suggest that these

multiple functions in Cars are the result of a strong correlation between a complex electronic structure [8–13] and a flexible geometry, which is easily tunable by the surrounding protein environment [14–17].

In this regard, one interesting example is the major peripheral light-harvesting complex (LHCII) of photosystem II in higher plants. LHCII is assembled into a trimeric form, that at each monomeric subunit binds 14 Chls (i.e., 8 Chl *a* and 6 Chl *b*) and 4 Cars, including 2 luteins in the sites L1 and L2, namely L1-Lut and L2-Lut. Identical in chemical structure but embedded in different protein pockets (see Fig. 1a), the two luteins in each monomer are known to feature distinct physical structures and to be spectrally distinct [4, 8, 14–20]. Indeed, the bright electronic excitation of lutein, which corresponds to a transition from the ground state to the second excited singlet state ( $S_0 \rightarrow S_2$ ), is ca. 600–700  $\text{cm}^{-1}$  red-shifted in L2-Lut with respect to that of L1-Lut [15, 17, 21].

Recent two-dimensional electronic spectroscopy (2DES) studies by Schlau-Cohen and co-workers [17] found that the different protein environment of the sites L1 and L2 in LHCII is able to tune the electronic properties of lutein,

Laura Pedraza-González and Davide Accomasso have contributed equally to this work.

✉ Benedetta Mennucci  
benedetta.mennucci@unipi.it

Laura Pedraza-González  
laura.pedraza@dcc.i.unipi.it

Davide Accomasso  
davide.accomasso@dcc.i.unipi.it

Lorenzo Cupellini  
lorenzo.cupellini@unipi.it

Giovanni Granucci  
giovanni.granucci@unipi.it

<sup>1</sup> Dipartimento di Chimica e Chimica Industriale, Università di Pisa, Via G. Moruzzi 13, 56124 Pisa, Italy

optimizing L2-Lut for light-harvesting. More specifically, they proposed that the  $S_2$  state of L1-Lut, together with the high-energy Soret band of the Chls, rapidly funnel energy to the lower-lying  $S_2$  state of L2-Lut, which serves as a direct donor state for excitation energy transfer (EET) to Chls. Such EET seems to be active only between luteins of the same monomeric subunit. In the same study, the authors identified a dark state of lutein, denoted as  $S_x$ , which was rapidly populated (in less than 20 femtoseconds) through a non-adiabatic transition originating solely from the  $S_2$  state of L2-Lut.  $S_x$  was proposed to facilitate the fast and efficient energy transfer from L2-Lut to chlorophyll. These findings imply that  $S_x$  is not present in the remaining three Carotenoids within LHCII but is instead exclusive to L2-Lut, underscoring its role in the light-harvesting process. On the other hand, femtosecond stimulated Raman spectroscopy (FSRS) experiments by Kennis and co-workers [20] have suggested that the  $S_2$  states of both luteins, L1-Lut and L2-Lut, are the main energy donors for EET to Chls. Remarkably, the authors excluded any appreciable energy transfer from  $S_2$  of L1-Lut to  $S_2$  of L2-Lut [20]. Instead, they proposed the  $S_1$  state of the high-energy lutein, L1-Lut, to serve as an additional channel contributing to light-harvesting, whereas the  $S_1$

state of the low-energy lutein, L2-Lut, is likely to be energetically lower than the chlorophyll states. Recently, Li and co-workers performed a computational investigation of the excitation energies of the two luteins in LHCII and evaluated the lutein-lutein energy transfer pathway [22]. Their quantum dynamics simulations suggest that the energy transfer between the two luteins can occur in conformations that place  $S_2$  states of L1-Lut and L2-Lut in resonance. Such results when combined with the measured marked difference in the  $S_2$  energy levels ( $700\text{ cm}^{-1}$ ) of the two luteins in LHCII would challenge the lutein-lutein energy transfer.

These somewhat contradictory findings emphasize that the debate about the involvement of carotenoids in the process of light-harvesting is not completely settled. In this context, molecular simulations could help building a thorough understanding of the factors controlling the excited-state properties of the luteins in LHCII and their excited state dynamics.

An investigation of the ultrafast photophysics of lutein in vacuum and in methanol solution was recently presented by some of us [23] by using a computational approach based on nonadiabatic excited-state dynamics. Briefly, we characterized the nature of the so-called  $S_x$  dark state in lutein as

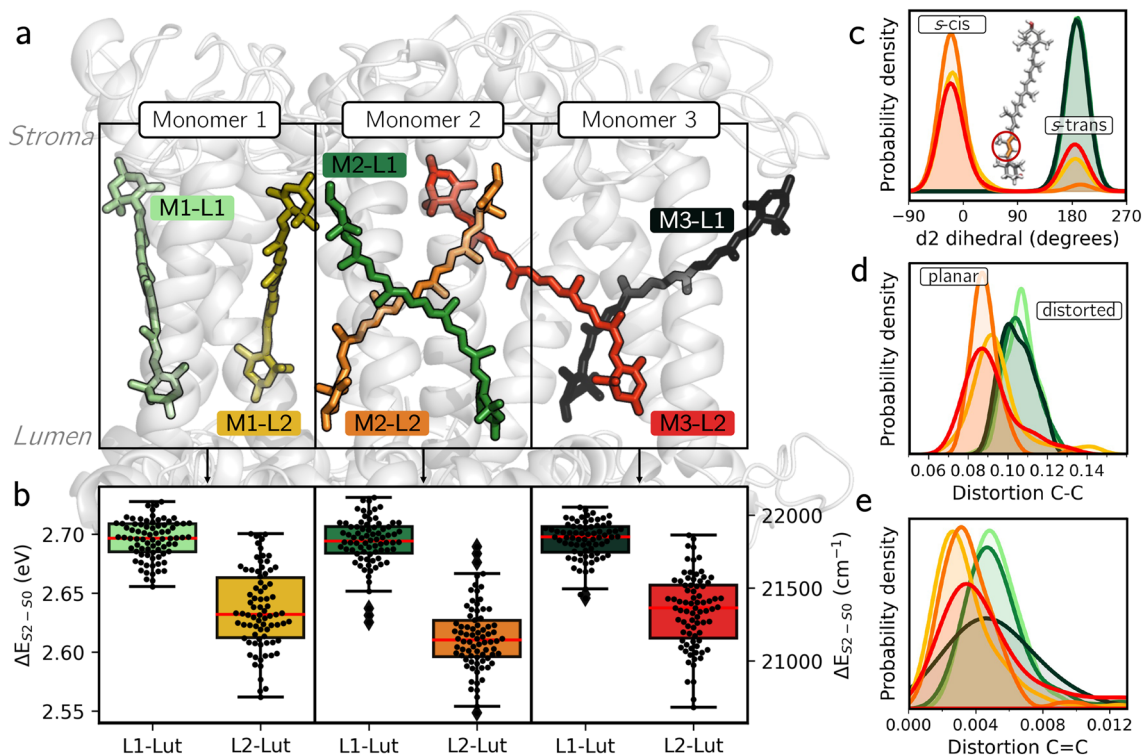


**Fig. 1** Structural and energetic properties of lutein in the sites L1 and L2 in trimeric LHCII. **a** Trimeric structure of LHCII, highlighting lutein pigments in the L1 and L2 sites of each monomer. **b** Box plot of the lutein  $S_2$  bright state, computed for the ground-state optimized structure of L1-Lut and L2-Lut of each monomer. Each box presents the median (horizontal red line), the first and third quartile (exten-

sion of the box), and the whiskers extend up to 1.5 IQR below and above the first and third quartile. Black points represent each computed value and black diamonds represent outliers. Distributions of **c** the lumenal dihedral  $d_2$ , and distortion around single **d** and double **e** bonds are also presented. Color labels in **b–e** are defined in **a**

an electronic state of  $B_u^-$  symmetry and found that  $S_x$  acts as an intermediate in the fast decay from the bright  $S_2$  state towards the dark  $S_1$  state of lutein both in vacuum and in solution.

Furthermore, some of us have recently extended the application of the same methodology as the excited state dynamics of another carotenoid (canthaxanthin) in the Orange Carotenoid Protein (OCP) [24]. Strikingly, these investigations suggested that the dark state  $S_x$  is equally involved in the ultrafast decay pathway of the  $S_2$  state of the two different carotenoids.

Although this methodology, which is based on the mixed quantum-classical surface hopping (SH) approach [25], has proven suitable for the study of single Cars, it lacks any description of inter-pigment EET processes. Persico and co-workers have recently reported a methodology for SH dynamics with the Frenkel exciton model, aimed at simulating the dynamics of multichromophoric systems [26], representing a good alternative for studying EET processes between pigments.

In this study, we employ QM/MM nonadiabatic dynamics with the SH approach to simulate the ultrafast dynamics of luteins within the L1 and L2 sites of the LHCII trimer, using both the single pigment and excitonic formulations (see Fig. S1). Comparing these two methods provides us with a comprehensive understanding that can be applied to explore some of the aspects that remain unresolved in the excited state decay of luteins in LHCII.

## 2 Methods

### 2.1 QM/MM DFT calculations

A set of 80 representative structures of LHCII trimer were extracted from a molecular dynamics (MD), previously reported by some of us [19, 27], which uses as a template the crystal structure of spinach trimeric LHCII (PDB code: 1RWT [28], chains C,H,E). Starting from such structures, ground-state ( $S_0$ ) geometry optimizations of both L1-Lut and L2-Lut were performed for each of the three monomers (see Fig. 1a), for a total of 480 calculations. An electrostatic embedding QM/MM method was used where the QM subsystem, defined by either L1-Lut or L2-Lut (98 atoms), was described at the DFT/B3LYP/6-31 G(d) level of theory whereas the rest of the system was modeled with the MM force field used in the MD, i.e., the AMBER ff14SB [29] and lipid14 [30] force fields for protein and lipids, respectively, and ad-hoc parameters for the pigments [31, 32]. In the geometry optimizations the MM layer defined by residues (i.e., Cars, Chls, amino acids, waters, etc.) within 6 Å of the QM part, was allowed to move whereas the rest of

the system was kept fixed. The optimized structures were employed to compute the  $S_0 \rightarrow S_2$  vertical excitation energy ( $\Delta E_{S_2-S_0}$ ) of both L1-Lut and L2-Lut, through a polarizable embedding QM/MM (QM/MMPol) [33]. Briefly, the QM/MMPol embedding treats the lutein of interest at the TD-DFT/M062X/6-31 G(d) level, whereas the rest of the system (i.e., LHCII trimer, lipids, and water molecules) is described classically as a set of point charges and induced dipoles. All calculations were performed with a locally modified version of the Gaussian package [34].

### 2.2 Single-chromophore surface hopping simulations

In the surface hopping (SH) nonadiabatic simulations, the electronic states of each lutein, either L1-Lut or L2-Lut, were computed using the semiempirical configuration interaction method with floating occupation molecular orbitals (FOMO-CI) [35, 36]. In the FOMO-CI calculations, we used the AM1 semiempirical model [37] with parameters specifically optimized for lutein [23]. Moreover, a Gaussian width for floating occupation of 0.1 Hartree was used, and we considered all the singly- and doubly-excited configurations (CISD) within an orbital active space of six electrons in nine molecular orbitals of  $\pi$  type (i.e., FOMO-CISD(6,9)). In the simulations, we employed a QM/MM electrostatic embedding scheme, in which the QM lutein is embedded in the MM protein environment of the LHCII trimer, which was described using the parameters employed in the MD (see above). In the QM/MM trajectories, we considered a subsystem of the LHCII trimer embedded in a solvated model membrane, as investigated in Refs. [20, 28]. Specifically, in the MM part we included only the pigments, protein residues, lipids, and water molecules within a distance of 25 Å from each lutein, and only the MM residues within 18 Å of lutein were allowed to move, while all the other MM atoms were kept frozen.

A subset of 18 out of the 80 representative structures of LHCII trimer were selected for the generation of independent ground-state QM/MM thermal trajectories for either L1-Lut or L2-Lut in each of the three monomers, for a total of 108 thermal trajectories (54 for each lutein) of 10 ps each. In the QM/MM thermal trajectories, we employed the van Gunsteren-Berendsen thermostat [38], which is based on Langevin's equation, and each trajectory was propagated using a time step of 0.5 fs, a temperature of 300 K, and a friction coefficient of  $5.0 \times 10^{13} \text{ s}^{-1}$  for all the atoms. The starting conditions for the SH trajectories, (i.e., the initial nuclear coordinates and velocities, and the starting electronic state) were sampled from the last 5 ps of each QM/MM thermal trajectory, using a procedure based on the dipole transition probability from the ground-state [39], within the excitation energy range of  $2.70 \pm 0.15 \text{ eV}$

for L1-Lut and  $2.65 \pm 0.15$  for L2-Lut. These energy ranges include most of the main band of the absorption spectrum of the corresponding lutein in LHCII trimer, computed along the QM/MM thermal equilibrations (see Fig. S3 and Fig. S4) In the SH simulations, we employed Tully's "fewest switches" algorithm [25], using a locally diabatic representation for the time evolution of the electronic wave function [36]. To account for quantum decoherence effects, we used the overlap decoherence correction (ODC) scheme [40], with the following parameters:  $\sigma = 1.0$  a.u. (Gaussian width) and  $S_{\min} = 5 \times 10^{-3}$  (minimum overlap threshold). A total of 551 and 558 QM/MM SH trajectories were propagated for 300 fs for L1-Lut and L2-Lut, respectively (see Table S2), with energy-conserving conditions (no thermostat), using a time step of 0.2 fs for the integration of both the nuclear degrees of freedom and the electronic ones. The six lowest singlet states were taken into account in the nonadiabatic SH dynamics. For each simulation time step, the population of each adiabatic electronic state  $i$  was computed as the fraction of SH trajectories running on the  $i$ -th PES. To characterize the physical nature of the electronic states in the SH simulations, we employed a diabaticization procedure previously devised in the framework of the FOMO-CI method [41], as described in Sect. S1.1.

All the semiempirical QM/MM simulations were performed using a development version of the MOPAC code [42], interfaced with the TINKER 6.3 package [43], in which the QM/MM semiempirical FOMO-CI technique and the SH method were implemented.

### 2.3 Excitonic surface hopping simulations

The excitonic SH simulations for L1-Lut and L2-Lut in LHCII were carried out using a methodology that combines the "fewest switches" SH algorithm with the Frenkel Exciton model [26]. In each QM/MM calculation, the electronic states of lutein were computed using the same semiempirical QM method employed in the single chromophore SH simulations, i.e., FOMO-CISD(6,9) with optimized AM1 parameters, and the electrostatic embedding scheme (see above). Moreover, in the MM part we included the residues within a distance of 25 Å from the dimer formed by L1-Lut and L2-Lut. The exciton couplings were computed as electrostatic interactions between transition atomic charges of each chromophore. To include, in an approximate fashion, the polarizable description of the environment (i.e., LHCII trimer) in the exciton model, all the exciton couplings were scaled by a factor of 0.67. Ten thermal trajectories were propagated for 10 ps in the ground state of the two luteins embedded in LHCII trimer, using the excitonic approach (see Sect. S1.2) and the Andersen thermostat [44], with a time step of 0.5 fs and a temperature of 300 K. The starting 10 structures for the thermal trajectories were selected from

the 80 representative structures of LHCII trimer mentioned above (see Sect. 2.1). At variance with the single-chromophore SH simulations, where thermal trajectories were performed on luteins from each of the three monomers, in these calculations we considered only luteins from monomer M2 (see Fig. 1a). The starting conditions for the SH excitonic trajectories were sampled from the last 5 ps of each ground-state thermal trajectory, using the same procedure employed for the single chromophore SH simulations (see Sect. 2.2 and Ref. [40]) with an excitation energy window of  $2.70 \pm 0.15$  eV. The excitonic SH simulations were performed using the "fewest switches" algorithm [25], with a locally diabatic representation for the time propagation of the electronic wave function [36], and the overlap decoherence correction (ODC) scheme [40], with the same parameters employed for the single chromophore simulations. A total of 306 excitonic SH trajectories were propagated for 600 fs, using a time step of 0.1 fs. For 137 SH trajectories L1-Lut is initially excited, while for the remaining 169 trajectories the initial excitation is localized on L2-Lut. A total of 11 electronic states were taken into account in the SH dynamics, including the 5 lowest singlet excited states of each of the two luteins and the ground state. Hereafter, we will label the states belonging to the excitonic basis as  $S_0S_0$ ,  $S_1S_0$ ,  $S_0S_1$ ,  $S_2S_0$ ,  $S_0S_2$ ,  $S_3S_0$ , and  $S_0S_3$ , where the excitations on the left and right correspond to L1-Lut and L2-Lut, respectively.

All the excitonic SH simulations were performed using the Newton-X package [45], modified to run exciton dynamics calculations, and a development version of the MOPAC code [42], interfaced with the TINKER 6.3 package [43], for the semiempirical QM/MM calculations.

## 3 Results and discussion

### 3.1 Structural and energetic properties of luteins L1 and L2

We first investigated how the lutein conformation, modulated by the L1 and L2 binding pockets (see Fig. 1a), tunes its electronic structure and thus its  $S_0 \rightarrow S_2$  absorption as experimentally observed in trimeric LHCII [14, 17].

We considered 80 representative structures extracted from an MD simulation [19, 27] of trimeric LCHII, and optimized their geometries at the QM/MM level (see Fig. 1a). Further details are provided in Sect. 2.1. Figure 1b illustrates the  $S_0 \rightarrow S_2$  vertical excitation energies ( $\Delta E_{S_2-S_0}$ ), computed for L1-Lut and L2-Lut, at the TD-DFT/M062X/6-31 G(d) MPMol level, along with the median values represented as horizontal red lines (see also Table S1). In each of the three monomers (i.e., M1, M2, and M3), L2-Lut indeed features lower excitation energies  $\Delta E_{S_2-S_0}$  than L1-Lut. The red shift, roughly quantified as the difference between the



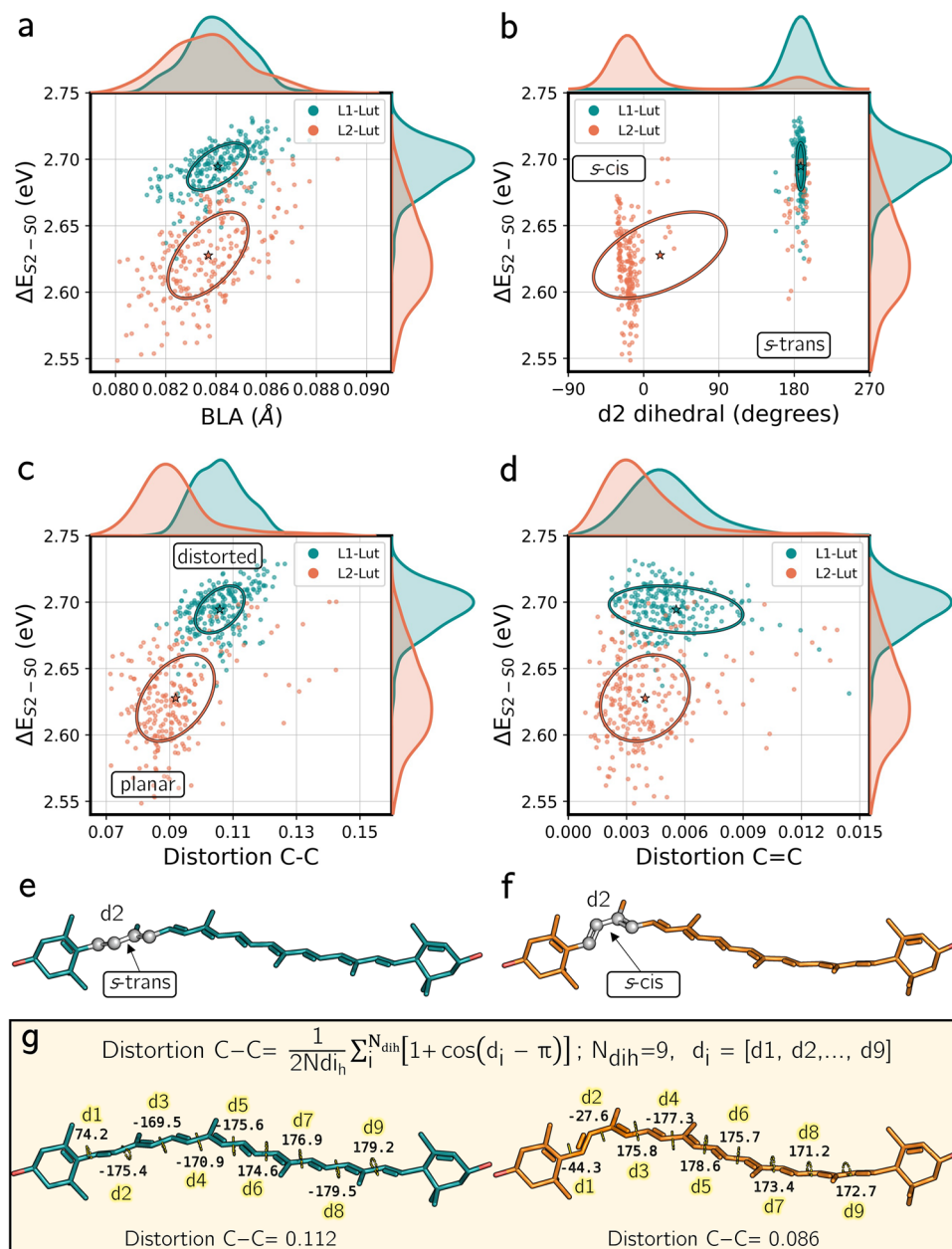
median values, amounts to about  $480\text{ cm}^{-1}$ ,  $650\text{ cm}^{-1}$ , and  $489\text{ cm}^{-1}$  for monomers M1, M2, and M3, respectively. These estimates are very close to the spectroscopic value of  $600\text{--}700\text{ cm}^{-1}$  [15, 17], suggesting that our QM/MM model faithfully reproduces the differences in the electronic structure of L1-Lut and L2-Lut in LHCII trimer.

To understand the origin of the red-shifted  $S_0 \rightarrow S_2$  absorption in L2-Lut, we examine the main structural features of lutein in LHCII. For both L1-Lut and L2-Lut, we considered the following geometrical parameters: (i) the bond-length alternation (BLA) of the  $\pi$ -conjugated chain (Fig. S5), which quantifies the average difference between the length of the C–C single bonds and that of C=C double

bonds, (ii) the conformation of the conjugated C–C single bonds (dihedrals d1–d9 in Fig. S6), and (iii) the distortion around the conjugated C–C and C=C bonds (see Fig. S7). Since the studied properties are very similar between the three monomers of LHCII, we pooled together the luteins of different monomers for all the following analyses.

Figure 2 displays, for each lutein, the correlation plots between each of the above mentioned geometrical parameters and the vertical excitation energy  $\Delta E_{S_2-S_0}$ . As shown in Fig. 2a, there is a clear correlation between the  $\Delta E_{S_2-S_0}$  excitation energies and the BLA, at least for each lutein separately. However, the BLA distributions for L1-Lut and L2-Lut are very similar, indicating that the BLA of lutein

**Fig. 2** Geometrical analysis of the optimized  $S_0$  geometries obtained for L1-Lut and L2-Lut sites, considering all three monomers. Scatter plot of  $\Delta E_{S_2-S_0}$  with respect to the **a** BLA, **b** dihedral d2, **c** distortion around single bonds and **d** distortion around double bonds. The mean of each system is indicated with a star. The covariance ellipse enclosing was constructed using one standard deviation ( $1\sigma$ ). Representative structures of **e** *s*-trans and **f** *s*-cis conformers of Lutein. **g** Schematic representation of the distortion C–C index and example on two representative structures of L1-Lut and L2-Lut extracted from the centers of the covariance ellipses of panel **c**.



is not significantly affected by the different protein binding sites L1 and L2 in LHCII. Therefore, this parameter cannot explain the difference between the two sites. On the other hand, important structural differences between L1-Lut and L2-Lut can be found by analyzing the dihedrals around the conjugated C–C bonds (d1–d9). As we can see from Fig. S6, the distributions for the first luminal dihedral angle (d1) of L1-Lut and L2-Lut are quite different. Specifically, L2-Lut presents two conformations for the dihedrals on the luminal side, suggesting a larger conformational freedom for this lutein. Similar observations have been reported by Liguori et al. for a different MD simulation of LHCII [16]. As observed in Fig. S6b (see also Fig. 1c), the conformational freedom is observed for the second C–C bond on the luminal side (d2). While L1-Lut exclusively assumes the *s*-trans conformation for this dihedral (see Fig. 2e), L2-Lut mainly populates the *s*-cis conformer (see Fig. 2f). We also note that *s*-cis conformations of lutein are associated with red-shifted  $\Delta E_{S_2-S_0}$  values. For the other C–C dihedrals (i.e., d3–d9) the two luteins always present a *s*-trans conformation (Fig. S6).

To investigate whether the different conformation around d2 can affect the geometry of the whole  $\pi$ -conjugated system of lutein, we computed a distortion index for both the C–C and the C=C conjugated bonds. According to our definition of the distortion index (Eq. S5), more distorted geometries are associated with larger values of the index. Figure 2g provides the definition of the “distortion C–C index”, as well as an example on how it is computed for a representative structure of *s*-trans and *s*-cis conformations of lutein. Interestingly, although for *s*-cis lutein d2 is less planar, the overall distortion is higher in *s*-trans lutein because of the contribution from all the other C–C torsions.

Figure 2c (see also Fig. 1d) reports the distributions of the C–C distortion for L1-Lut and L2-Lut in LHCII trimer. As we can see, L1-Lut assumes geometries with larger C–C distortion than L2-Lut. This indicates that the *s*-cis conformation of L2-Lut allows the carotenoid to keep a more planar (i.e., less distorted) molecular geometry inside the protein binding pocket, compared to the *s*-trans L1-Lut. The C–C distortion is weakly correlated with the excitation energy in both L1-Lut and L2-Lut, and especially explains the difference between the two luteins. On the other hand, the distributions of the C=C distortion for L1-Lut and L2-Lut (Fig. 1e) are quite similar, with a slightly larger C=C distortion for L1-Lut. This suggests that the twisting around the conjugated C=C bonds of lutein in LHCII trimer is only slightly affected by the different conformation around d2.

In summary, we have identified important structural differences between L1-Lut and L2-Lut, the main difference being the conformation around the second dihedral angle in the luminal side (d2, Fig. 1c). Specifically, while L1-Lut only populates the *s*-trans ground-state conformer, L2-Lut mainly exists in the *s*-cis conformation around d2. This

structural difference significantly affects the  $\pi$ -conjugated system of the two luteins, with a larger distortion around the conjugated C–C bonds for L1-Lut, compared to L2-Lut. This indicates that the *s*-cis conformation allows a more planar lutein structure than the *s*-trans. In turn, a more distorted *s*-trans structure explains the higher excitation energy for L1-Lut (see Fig. 2).

### 3.2 Ultrafast decay pathway of the $S_2$ state of lutein: L1 versus L2

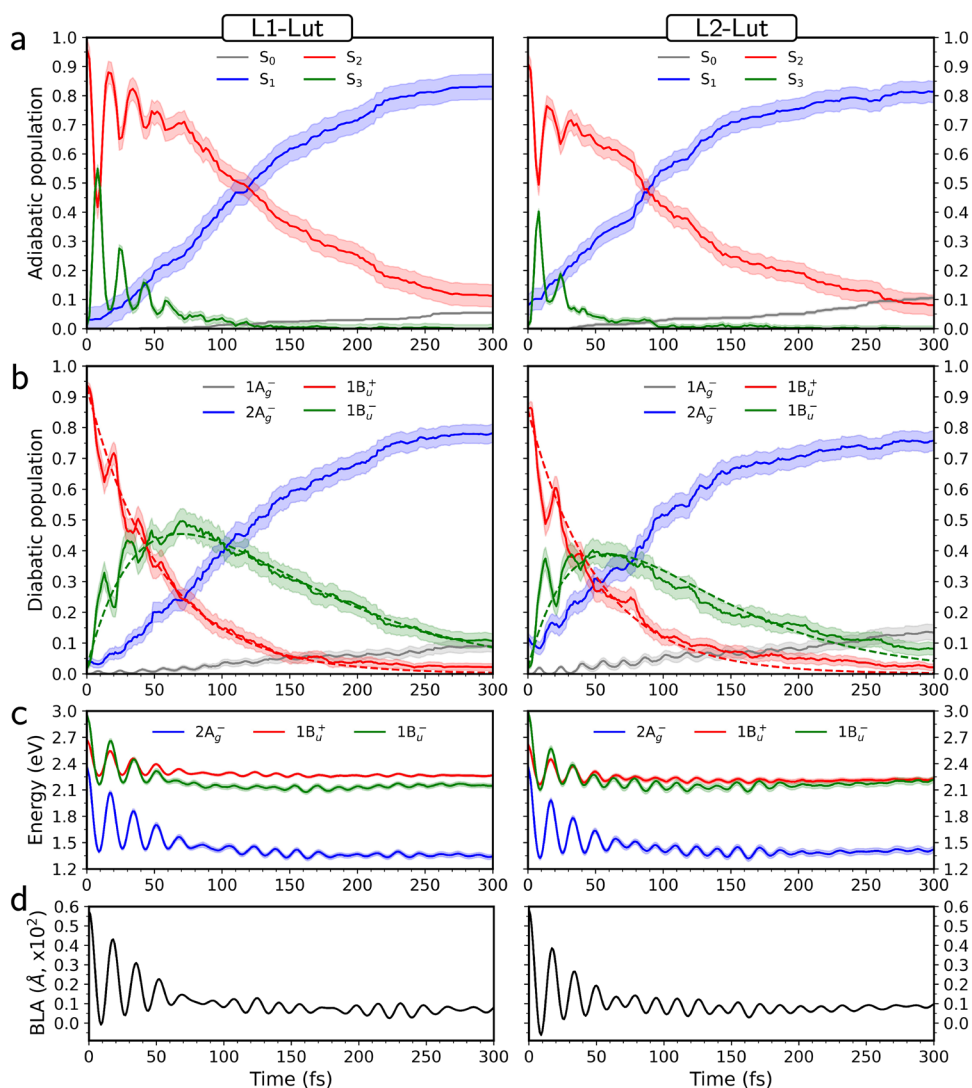
Our aim is now to investigate whether the energetic and structural differences of L1-Lut and L2-Lut, discussed in Sect. 3.1, can lead to different ultrafast excited-state dynamics. As detailed in Sect. 2.2, we employed the SH approach using a QM/MM electrostatic embedding scheme in which the QM subsystem includes one lutein molecule, either L1-Lut or L2-Lut, described by a semiempirical configuration interaction technique.

To verify if the energetics and structural differences between L1-Lut and L2-Lut, presented in Sect. 3.1, are preserved in our QM/MM semiempirical calculations, we analyzed the ground-state structural ensemble from which the initial conditions for the SH simulations are sampled. We computed the vertical excitation energy,  $\Delta E_{S_2-S_0}$ , as well as the BLA coordinate and the distortion index around the conjugated C–C bonds of lutein (Fig. S8). Although here the distributions are broader because they include thermal effects, the results of Sect. 3.1 are confirmed. Specifically, the excitation energy distribution for L2-Lut is red-shifted compared to L1-Lut, and L2-Lut shows a generally lower C–C distortion than L1-Lut (Fig. S8b), whereas the BLA distributions for the two luteins are very similar (Fig. S8a).

We first followed the adiabatic populations of the first three excited states upon excitation (Fig. 3a). The excitation initially populates the  $S_2$  bright state, and the excited-state evolution is similar for the two luteins. Within the first 50 fs, we observe rapid oscillations of the  $S_2$  and  $S_3$  populations, indicating a back-and-forth population exchange between these two states. These oscillations are more pronounced and last longer for L1-Lut than L2-Lut. At longer times (> 50 fs), we see a rise in the population of the lower-lying  $S_1$  state, which is the most populated state at the end of the simulations (300 fs).

At any time, an adiabatic state (e.g.  $S_2$ ) could have different character depending on the geometry or even be a mixture of states with different character (the diabatic states). To better characterize the physical nature of the four low-lying adiabatic states of lutein during the ultrafast dynamics reported in Fig. 3a, we introduce a diabatic representation. In practice, we assign the adiabatic state populations to the diabatic states according to the squared projection  $|\langle \Psi_i^{(D)} | \Psi_k^{(A)} \rangle|^2$  between the adiabatic state  $k$  and each diabatic

**Fig. 3** Ultrafast single-chromophore excited-state dynamics of luteins in the sites L1 and L2 in trimeric LHCII. Adiabatic **a** and diabatic **b** state populations as functions of time obtained from the simulations of excited-state dynamics for lutein L1 (left) and L2 (right) in LHCII. **c** Energies (eV) of the three low-lying diabatic excited states relative to the diabatic ground state ( $1A_g^-$ ) and **d** bond-length alternation (BLA, Å) as functions of time are also shown. The reported results are obtained by averaging over all trajectories (all monomers, see Figs. S9 and S10) and time intervals of 1 fs. Shaded regions mark two bootstrap standard error obtained from 1500 samples. Dashed lines represent the fitting functions of diabatic populations



state  $i$ . More specifically, we use four diabatic states which are defined so that they maximally resemble the four lowest adiabatic states of an isolated lutein ( $S_0$ - $S_3$ ) at its ground state minimum geometry. Here, they will be indicated using their (pseudo)symmetry, i.e.,  $1A_g^-$ ,  $2A_g^-$ ,  $1B_u^+$ , and  $1B_u^-$  [23, 24]. All the details about the diabaticization procedure are provided in Sect. S1.1.

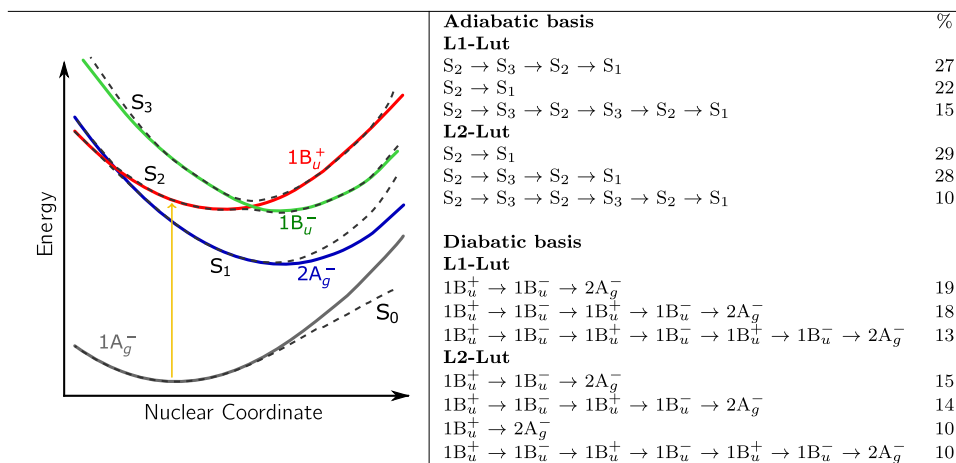
Figure 3b displays the diabatic state population dynamics for L1-Lut (left panel) and L2-Lut (right panel). Also here, a similar evolution is obtained for both luteins. The  $1B_u^+$  bright state initially excited rapidly transfers its population to the  $1B_u^-$  dark state. The very fast population rise of  $1B_u^-$ , which occurs in the first  $\sim 50$  fs of the simulations, is then followed by the decay of  $1B_u^-$ , which transfers its population mainly to  $2A_g^-$ .

As listed in Table 1, for both luteins the two main relaxation mechanisms involve the formation of the  $1B_u^-$  state. In particular, they are (i)  $1B_u^+ \rightarrow 1B_u^- \rightarrow 2A_g^-$  and (ii)  $1B_u^+ \rightarrow 1B_u^- \rightarrow 1B_u^+ \rightarrow 1B_u^- \rightarrow 2A_g^-$ , and account for 37% and

29% of the SH trajectories for L1-Lut and L2-Lut, respectively. The direct  $1B_u^+ \rightarrow 2A_g^-$  conversion is observed in only 6% and 10% of the SH trajectories for L1-Lut and L2-Lut, respectively, and therefore represents a minor decay pathway for both luteins. Notably, when the relaxed  $1B_u^-$  state decays into  $2A_g^-$ , the two diabatic states correspond to  $S_2$  and  $S_1$ , respectively; therefore, this transition is registered as  $S_2 \rightarrow S_1$  in the adiabatic basis. This picture essentially resembles the ultrafast evolution simulated for lutein in a methanol solution [23].

In Fig. 3c, d we show the energies of the three lowest diabatic excited states and the bond-length alternation (BLA) coordinate, averaged over all of the SH trajectories, as functions of time. During the ultrafast dynamics, we observe high-frequency oscillations of the diabatic state energies, which are caused by the oscillations of the BLA coordinate. In the first  $\sim 50$  fs of the relaxation dynamics, the  $1B_u^+$  and  $1B_u^-$  undergo multiple energy swaps. At longer times, the  $1B_u^-$  dark state lies most often energetically below  $1B_u^+$  for

**Table 1** Left panel: Schematic representation of the Potential Energy Surfaces of lutein along an effective nuclear coordinate for the adiabatic states ( $S_1$ – $S_3$ , dashed lines) and diabatic states ( $1A_g^-$ ,  $2A_g^-$ ,  $1B_u^+$ ,  $1B_u^-$ , solid lines); Right panel: Main relaxation pathways in both the



both L1-Lut and L2-Lut, with a larger average energy gap between  $1B_u^-$  and  $1B_u^+$  for L1-Lut. Throughout the ultrafast dynamics of both luteins, we observe first a strong oscillation of the BLA coordinate. After  $\sim 100$  fs, the BLA is substantially decreased, corresponding to the elongation of the C=C bonds and the shortening of the C–C bonds of the conjugated chain of lutein.

To determine the characteristic times of the excited-state transitions, we fitted the diabatic state populations using the simple kinetic model  $1B_u^+ \rightarrow 1B_u^- \rightarrow 2A_g^- + 1A_g^-$ , with fixed rate constants (see Sect. S1.3 for details). As shown in Fig. 3b, the fitting functions (Eq. S4), reported by dashed lines, well describe the population dynamics of the two luteins. We obtained the following time constants:  $\tau_{2x} = 54$  fs (L1-Lut) and 51 fs (L2-Lut) for the  $1B_u^+ \rightarrow 1B_u^-$  transition, and  $\tau_{x1} = 96$  fs (L1-Lut) and 75 fs (L2-Lut) for  $1B_u^- \rightarrow 2A_g^- + 1A_g^-$ . These extracted times further confirm that in our simulations the ultrafast population dynamics of L1-Lut and L2-Lut in LHCII are very similar.

As shown previously [23, 24, 46],  $1B_u^-$  can be identified with the spectroscopically observed  $S_x$  dark state. Our simulations indicate that also in LHCII the ultrafast  $S_2 \rightarrow S_1$  internal conversion is mediated by the  $S_x$  ( $1B_u^-$ ) state. Our extracted lifetimes for the  $S_2$  ( $1B_u^+$ ) and  $S_x$  ( $1B_u^-$ ) states, i.e.,  $\tau_{2x} = 51$ –54 fs and  $\tau_{x1} = 75$ –96 fs, are of the same order of magnitude as those reported for lutein in gas-phase [23], solution [23, 46, 47] and LHCII [17] (see Table S3).

Our simulations indicate that the carotenoid  $S_x$  state is not exclusive of L2-Lut, as suggested by Schlau-Cohen and co-workers [17], but it is also involved in the excited-state relaxation dynamics of L1-Lut in LHCII. What is more, the relaxation dynamics is remarkably similar in the two luteins. Assuming that the model here used

adiabatic and diabatic basis obtained in the Excited-State simulations of Lutein L1 and L2 in LHCII. The % indicates the percentage number of SH trajectories showing that specific pathway. Only pathways with % equal or larger than 10 are reported

contains all the needed components to detect any possible difference in behavior between the two luteins, a possible explanation for this discrepancy is that the ultrafast dynamics is indeed the same in the two luteins, but the  $S_x$  state is detected only in L2-Lut. The only difference between the two luteins is that in L2-Lut the energies of  $S_2$  ( $1B_u^+$ ) and  $S_x$  ( $1B_u^-$ ) stay remarkably close throughout the first 300 fs of excited-state dynamics (see Fig. 3c). This may allow the two states to mix more efficiently, allowing  $S_x$  to borrow dipole strength from  $1B_u^+$ . Another possibility is that  $S_x$  is not detected in L1-Lut because of an ultrafast energy transfer to L2-Lut. This could only occur if the energy transfer is faster than the internal conversion to  $S_x$ . We will explore this possibility in the next section.

### 3.3 Excitation energy transfer

Here we employ two different theoretical approaches to evaluate the excitation energy transfer between the two  $S_2$  states of luteins in LHCII. As a first approach, we estimated the EET rate in the framework of Förster theory, which only requires calculating the electronic coupling and the spectral overlap between donor emission and acceptor absorption. This approach assumes weak coupling between the  $S_2$  states of each Lut, and ignores the nonadiabatic dynamics within each pigment. However, it treats quantum mechanically the vibrational degrees of freedom of the two interacting pigments [48]. As a second approach, we employed the SH method combined with a Frenkel exciton model [26]. Such methodology allows to simulate the nonadiabatic dynamics of multichromophoric systems in which excitation energy transfer can occur. As



such, it treats the EET and internal conversion processes on the same grounds.

### 3.3.1 Förster model

As the two involved excitations are bright and the center-to-center distance between L1-Lut and L2-Lut, within the same monomeric unity, is about 13 Å, we can safely approximate the electronic coupling with its Coulomb contribution. To compute the Coulomb coupling between the  $S_2$  bright states of L1-Lut and L2-Lut, we employed the same QM/MMPol model used in Ref. [49]: a transition charge approximation to represent the QM transition densities of the luteins [50], and an atomistic and polarizable classical model to describe the environment atoms. Our calculated value for the coupling between the two luteins in the same monomer ( $75 \text{ cm}^{-1}$ ) is very close to that previously obtained using transition density cube (TDC) calculations [51] (ca.  $81 \text{ cm}^{-1}$ ), but almost twice the value reported by Li and co-workers [22]. We calculated the spectral overlap using the time-domain expression in the spectral density formalism (see Sect. S3) [48]. The parameters of the spectral density were determined by a fitting of the absorption spectrum of lutein.

To better understand the effectiveness of the energy transfer between the two luteins we have calculated the  $S_2$  (L1-Lut)  $\rightarrow$   $S_2$ (L2-Lut) Förster EET time constant as a function of the energy gap (see Fig. S11). As observed, the EET time is raised when the energy gap is ca.  $700\text{--}800 \text{ cm}^{-1}$ , reaching a maximum value of about 2 ps and never going below 1 ps. This value is more than one order of magnitude higher than the 60 fs estimated with ultrabroadband 2D electronic spectroscopy [17, 21] and suggests that an ultrafast energy transfer between the  $S_2$  bright states of the two luteins in the LHCII trimer does not occur. These conclusions are in line with the femtosecond stimulated Raman spectroscopy study of Kennis and co-workers [20], who found no appreciable energy transfer from L1-Lut to L2-Lut.

### 3.3.2 SH dynamics with the Frenkel exciton model

To better investigate the interplay between inter-pigment EET and intra-pigment excited-state dynamics, we employed the SH method combined with a Frenkel exciton model [26], as described in Sect. 2.3. In this way, we include atomistically the nuclear motion of the two luteins, as well as of the protein, in the multichromophoric excited-state dynamics.

First, we calculated the multichromophoric absorption spectrum from the ground-state thermal trajectories (Fig. S12). The main band of the spectrum approximately corresponds to the sum of the bands of the  $S_2$  bright states of the two luteins. This indicates that the excitonic mixing of the two  $S_2$  excitations is very small and does not cause any

important shift in the absorption spectrum of the two luteins. We note that the red-shifting of L2-Lut with respect to L1-Lut, discussed above for both (TD-)DFT MMPol (Sect. 3.1) and single-chromophore SH (Sect. 3.2) calculations, is also preserved in these simulations.

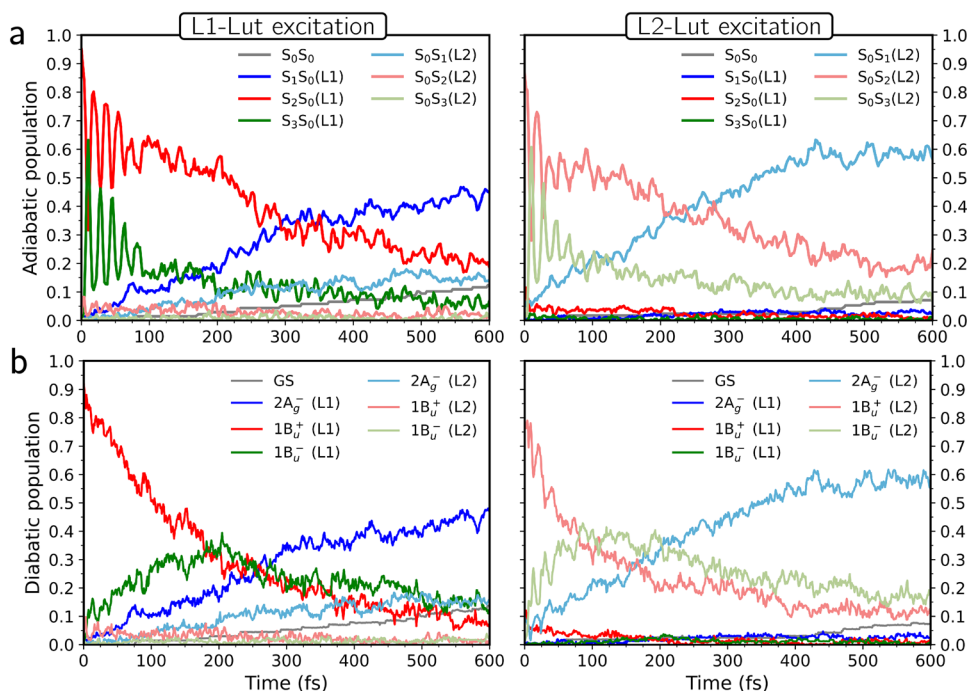
As the mixing of the two  $S_2$  bright states is negligible, we can separate the SH trajectories where L1-Lut is initially excited from those with initial excitation of L2-Lut. This procedure also allows us to mimic experimental conditions where each lutein in LHCII is selectively excited [20]. The state population dynamics obtained from these two sets of SH trajectories are shown in Fig. 4.

When L1-Lut is excited (Fig. 4, panels a and b, left), most of the population dynamics involve the excited states of L1-Lut. In particular, in the adiabatic basis (Fig. 4a, left), we observe an initial exchange of population between  $S_2$  and  $S_3$  of L1-Lut, which is followed by the decay of these two states mainly to the lower-lying  $S_1$  state of the same chromophore. In the diabatic basis (Fig. 4b, left), the transfer of population from the photo-generated  $1B_u^+$  state to the intermediate  $1B_u^-$  state of L1-Lut precedes the slower decay of the latter state to  $2A_g^-$ . A similar population dynamics is obtained when L2-Lut is excited (Fig. 4, panels a and b, right), confirming negligible differences between the ultrafast  $S_2$  decay of both luteins. Indeed, for both L1-Lut and L2-Lut excitations, the time evolutions of the populations computed with the excitonic approach are qualitatively very similar to those we obtained for the two separate luteins (Sect. 3.2, Fig. 3).

It is worth noting that the dynamics in the exciton model seems slower than the single-chromophore dynamics reported in Sect. 3.2. This is due to the different treatment of uphill transitions, which are favored in the simulations performed according to the Frenkel exciton model, ultimately resulting in a reduced downhill relaxation rate. Nonetheless, the mechanism of relaxation remains the same as in the single-chromophore SH simulations.

The population dynamics described above show no evident transfer from the  $S_2$  ( $1B_u^+$ ) bright state of L1-Lut to the  $S_2$  ( $1B_u^+$ ) bright state of L2-Lut. Indeed, when L1-Lut is excited, there is no significant increase in the  $S_2$  ( $1B_u^+$ ) population of L2-Lut throughout the simulation time. Curiously though, we could detect a rise in the population of the  $S_1$  ( $2A_g^-$ ) state of L2-Lut in the simulations started from an excited L1-Lut. The opposite does not occur, namely the  $S_1$  state of L1-Lut is not populated upon excitation of L2-Lut. The initial rise of the L2-Lut  $S_1$  population is compatible with a transfer time slower than 1 ps. These results exclude the energy transfer into  $S_2$  of L2-Lut from the higher-lying state  $S_2$  of L1-Lut and essentially confirm the picture obtained using Förster theory (Sect. 3.3.1).

**Fig. 4** Ultrafast multichromophore excited-state dynamics of luteins in the sites L1 and L2 in trimeric LHCII. Populations of adiabatic localized excitations **a** and diabatic states **b** as functions of time obtained from the SH dynamics with the Frenkel exciton model, divided according to the initial excitation either on L1-Lut (left) or L2-Lut (right). The reported results are obtained by averaging over all trajectories (monomer M2) and time intervals of 0.1 fs



On the other hand, it is worth noticing that, in agreement with the SH single-chromophore simulations discussed in Sect. 3.2, the SH excitonic model confirms the formation of the  $1B_u^-$  ( $S_x$ ) dark state for both luteins in the sites L1 and L2 (see Fig. 4b). Therefore, we can conclude from our calculations that the formation of the  $S_x$  dark state in LHCII is not exclusive to the L2 site but is also present in L1.

## 4 Conclusions

In this work, we have investigated how the different protein pockets at the L1 and L2 sites of the trimeric LHCII tune the electronic structure of the embedded lutein, and how this reflects on the ultrafast dynamics upon excitation of the bright  $S_2$  state. By combining MD and QM/MM calculations, we found that the red-shift of  $S_0 \rightarrow S_2$  absorption in L2-Lut is caused by relevant structural differences between L1-Lut and L2-Lut. While the former exclusively populates the *s*-trans ground-state conformation around the second dihedral angle in the luminal side, the latter mainly populates the *s*-cis conformation. The *s*-cis preference of L2-Lut allows for a more planar geometry of the  $\pi$ -conjugated backbone, which results in an increased degree of delocalization and a reduced excitation energy.

Notwithstanding the difference in the geometry and electronic structure of L1-Lut and L2-Lut, surface hopping simulations reveal that the two luteins present analogous ultrafast dynamics upon excitation. As previously suggested for lutein in solution [23], the bright  $S_2$  ( $1B_u^+$ ) state

quickly decays (in  $\sim 50$  fs) into the dark intermediate  $S_x$  ( $1B_u^-$ ), eventually ending up in the  $S_1$  ( $2A_g^-$ ) state. Remarkably, consistent results are obtained in a multichromophoric excited-state dynamics scheme, i.e., the surface hopping method combined with a Frenkel exciton model. These results imply that, at variance with spectroscopic findings, the  $S_x$  state is involved in the excited-state relaxation dynamics of both L2-Lut and L1-Lut.

On the other hand, we have investigated the experimentally debated EET from the  $S_2$  state of L1-Lut to the lower-lying  $S_2$  state of L2-Lut. By using Förster theory we predicted that EET is more than one order of magnitude slower than what was experimentally measured (ca. 60 fs), excluding an ultrafast EET between the two luteins. These results were confirmed by analyzing the multichromophoric excited-state dynamics upon selective excitation of L1-Lut, where no evident transfer from the bright state of L1-Lut to the bright state of L2-Lut was observed.

Although in this paper we focused on the role of the two luteins present in LHCII, we remark that the general picture of the energy transfer pathways in this protein is much more complex. As a matter of fact, the three types of carotenoids in LHCII, i.e., lutein, neoxanthin, and violaxanthin, absorb energy in similar windows, and excitation of multiple carotenoids at once is possible [20]. Furthermore, EET to chlorophylls, from  $S_2$  or  $S_x$ , is fast and competitive with the internal conversion of these states. There are still controversies regarding the specific role of not only the two luteins studied in this work, but also of

the other two embedded carotenoids [4, 14, 19, 20, 52–55]. Therefore, gaining insights into structural, electronic, and dynamic information from all the Cars, as well as their interaction with the embedded Chls, is still a hot topic from both experimental and theoretical points of view.

## 5 Supplementary information

Details on surface hopping simulations: diabaticization analysis, description of SH exciton models, and fitting of the state populations; definition of index of distortion of the lutein  $\pi$ -conjugated chain; and calculation of  $S_2$  (L1-Lut) $\rightarrow S_2$  (L2-Lut) EET Förster rates. Supplementary tables and figures are also provided.

**Supplementary Information** The online version contains supplementary material available at <https://doi.org/10.1007/s43630-023-00518-x>.

**Acknowledgements** L.P.-G., D.A., L.C., and B.M. acknowledge funding by the European Research Council, under the Grant ERC-AdG 786714 (LIFETIME). The authors acknowledge Edoardo Cignoni for support in the construction of the model for computing Coulomb coupling.

**Data availability** All relevant data are within the manuscript and its Supplementary files.

## Declarations

**Conflict of interest** The authors declared that they have no conflict of interest in this work.

**Open Access** This article is licensed under a Creative Commons Attribution 4.0 International License, which permits use, sharing, adaptation, distribution and reproduction in any medium or format, as long as you give appropriate credit to the original author(s) and the source, provide a link to the Creative Commons licence, and indicate if changes were made. The images or other third party material in this article are included in the article's Creative Commons licence, unless indicated otherwise in a credit line to the material. If material is not included in the article's Creative Commons licence and your intended use is not permitted by statutory regulation or exceeds the permitted use, you will need to obtain permission directly from the copyright holder. To view a copy of this licence, visit <http://creativecommons.org/licenses/by/4.0/>.

## References

- Ruban, A. V., et al. (2007). Identification of a mechanism of photoprotective energy dissipation in higher plants. *Nature*, *450*, 575–578.
- Polivka, T., & Frank, H. A. (2010). Molecular factors controlling photosynthetic light harvesting by carotenoids. *Accounts of Chemical Research*, *43*, 1125–1134.
- Hashimoto, H., Sugai, Y., Urugami, C., Gardiner, A. T., & Cogdell, R. J. (2015). Natural and artificial light-harvesting systems utilizing the functions of carotenoids. *Journal of Photochemistry and Photobiology C: Photochemistry Reviews*, *25*, 46–70.
- Croce, R., Müller, M. G., Bassi, R., & Holzwarth, A. R. (2001). Carotenoid-to-chlorophyll energy transfer in recombinant major light-harvesting complex (LHCII) of higher plants. I. Femtosecond transient absorption measurements. *Biophysical Journal*, *80*, 901–915.
- Caffarri, S., Croce, R., Breton, J., & Bassi, R. (2001). The major antenna complex of photosystem II has a xanthophyll binding site not involved in light harvesting. *Journal of Biological Chemistry*, *276*, 35924–35933.
- Mozzo, M., Dall'Osto, L., Hienerwadel, R., Bassi, R., & Croce, R. (2008). Photoprotection in the antenna complexes of photosystem II. *Journal of Biological Chemistry*, *283*, 6184–6192.
- Pedraza-González, L., Cignoni, E., D'Ascenzi, J., Cupellini, L., & Mennucci, B. (2023). How the pH controls photoprotection in the light-harvesting complex of mosses. *Journal of the American Chemical Society*, *145*, 7482–7494.
- Ruban, A. V., Pascal, A. A., Robert, B., & Horton, P. (2001). Configuration and dynamics of xanthophylls in light-harvesting antennae of higher plants: spectroscopic analysis of isolated light-harvesting complex of photosystem II and thylakoid membranes. *Journal of Biological Chemistry*, *276*, 24862–24870.
- Polívka, T., & Sundström, V. (2004). Ultrafast dynamics of carotenoid excited States—from solution to natural and artificial systems. *Chemical Reviews*, *104*, 2021–71.
- Polívka, T., & Sundström, V. (2009). Dark excited states of carotenoids: Consensus and controversy. *Chemical Physics Letters*, *477*, 1–11.
- Schenk, E. R., et al. (2014). Direct observation of differences of carotenoid polyene chain cis/trans isomers resulting from structural topology. *Analytical Chemistry*, *86*, 2019–2024.
- Hashimoto, H., Urugami, C., Yukihira, N., Gardiner, A. T., & Cogdell, R. J. (2018). Understanding/unravelling carotenoid excited singlet states. *Journal of the Royal Society Interface*, *15*, 20180026.
- Fiedor, L., Dudkowiak, A., & Pilch, M. (2019). The origin of the dark s1 state in carotenoids: A comprehensive model. *Journal of the Royal Society Interface*, *16*, 20190191.
- Yan, H., Zhang, P., Wang, C., Liu, Z., & Chang, W. (2007). Two lutein molecules in LHCII have different conformations and functions: Insights into the molecular mechanism of thermal dissipation in plants. *Biochemical and Biophysical Research Communications*, *355*, 457–463.
- Mendes-Pinto, M. M., et al. (2013). Mechanisms underlying carotenoid absorption in oxygenic photosynthetic proteins. *Journal of Biological Chemistry*, *288*, 18758–18765.
- Liguori, N., et al. (2017). Different carotenoid conformations have distinct functions in light-harvesting regulation in plants. *Nature Communications*, *8*, 1994.
- Son, M., Pinnola, A., Bassi, R., & Schlau-Cohen, G. S. (2019). The electronic structure of lutein 2 is optimized for light harvesting in plants. *Chem*, *5*, 575–584.
- Ruban, A. V., Pascal, A. A., & Robert, B. (2000). Xanthophylls of the major photosynthetic light-harvesting complex of plants: Identification, conformation and dynamics. *FEBS Letters*, *477*, 181–185.
- Cupellini, L., Calvani, D., Jacquemin, D., & Mennucci, B. (2020). Charge transfer from the carotenoid can quench chlorophyll excitation in antenna complexes of plants. *Nature Communications*, *11*, 1–8.
- Artes Vivancos, J. M., et al. (2020). Unraveling the excited-state dynamics and light-harvesting functions of xanthophylls in light-harvesting complex II using femtosecond stimulated Raman spectroscopy. *Journal of the American Chemical Society*, *142*, 17346–17355.

21. Son, M., Hart, S. M., & Schlau-Cohen, G. S. (2021). Investigating carotenoid photophysics in photosynthesis with 2D electronic spectroscopy. *Trends in Chemistry*, *3*, 733–746.
22. Li, J., Zeng, T., Zhai, Y., Qu, Z., Li, H., et al. (2023). Intermolecular resonance energy transfer between two lutein pigments in light-harvesting complex ii studied by Frenkel exciton models. *Physical Chemistry Chemical Physics*, *25*, 24636–24642.
23. Accomasso, D., Arslançan, S., Cupellini, L., Granucci, G., & Mennucci, B. (2022). Ultrafast excited-state dynamics of carotenoids and the role of the  $S_X$  state. *The Journal of Physical Chemistry Letters*, *13*, 6762–6769.
24. Arcidiacono, A., Accomasso, D., Cupellini, L., & Mennucci, B. (2023). How orange carotenoid protein controls the excited state dynamics of canthaxanthin. *Chemical Science*, *14*, 11158–11169.
25. Tully, J. C. (1990). Molecular dynamics with electronic transitions. *The Journal of Chemical Physics*, *93*, 1061–1071.
26. Gil, E. S., Granucci, G., & Persico, M. (2021). Surface hopping dynamics with the Frenkel exciton model in a semiempirical framework. *Journal of Chemical Theory and Computation*, *17*, 7373–7383.
27. Balevičius, V., Jr., et al. (2017). Fine control of chlorophyll-carotenoid interactions defines the functionality of light-harvesting proteins in plants. *Scientific Reports*, *7*, 13956.
28. Liu, Z., et al. (2004). Crystal structure of spinach major light-harvesting complex at 2.72 Å resolution. *Nature*, *428*, 287–292.
29. Maier, J. A., et al. (2015). ff14SB: Improving the accuracy of protein side chain and backbone parameters from ff99SB. *Journal of Chemical Theory and Computation*, *11*, 3696–3713.
30. Dickson, C. J., et al. (2014). Lipid14: The amber lipid force field. *Journal of Chemical Theory and Computation*, *10*, 865–879.
31. Zhang, L., Silva, D.-A., Yan, Y., & Huang, X. (2012). Force field development for cofactors in the photosystem II. *Journal of Computational Chemistry*, *33*, 1969–1980.
32. Prandi, I. G., Viani, L., Andreussi, O., & Mennucci, B. (2016). Combining classical molecular dynamics and quantum mechanical methods for the description of electronic excitations: The case of carotenoids. *Journal of Computational Chemistry*, *37*, 981–991.
33. Curutchet, C., et al. (2009). Electronic energy transfer in condensed phase studied by a polarizable QM/MM model. *Journal of Chemical Theory and Computation*, *5*, 1838–1848.
34. Frisch, M. J., et al. (2016). *Gaussian 16 revision A03*. Wallingford, CT: Gaussian Inc.
35. Granucci, G., & Toniolo, A. (2000). Molecular gradients for semiempirical CI wavefunctions with floating occupation molecular orbitals. *Chemical Physics Letters*, *325*, 79–85.
36. Granucci, G., Persico, M., & Toniolo, A. (2001). Direct semiclassical simulation of photochemical processes with semiempirical wave functions. *The Journal of Chemical Physics*, *114*, 10608–10615.
37. Dewar, M. J. S., Zoebisch, E. G., Healy, E. F., & Stewart, J. J. P. (1985). AM1: A new general purpose quantum mechanical molecular model. *Journal of the American Chemical Society*, *107*, 3902–3909.
38. van Gunsteren, W. F., & Berendsen, H. J. C. (1982). Algorithms for Brownian dynamics. *Molecular Physics*, *45*, 637–647.
39. Persico, M., & Granucci, G. (2014). An overview of nonadiabatic dynamics simulations methods, with focus on the direct approach versus the fitting of potential energy surfaces. *Theoretical Chemistry Accounts*, *133*, 1526/1–1526/28.
40. Granucci, G., & Persico, M. A. Z. (2010). Including quantum decoherence in surface hopping. *The Journal of Chemical Physics*, *133*, 134111/1–134111/9.
41. Accomasso, D., Persico, M., & Granucci, G. (2019). Diabatization by localization in the framework of configuration interaction based on floating occupation molecular orbitals (FOMO-CI). *ChemPhotoChem*, *3*, 933–944.
42. Stewart, J. J. P. (2002). *MOPAC2002*. Tokyo: Fujitsu Limited.
43. Ponder, J. W. (Feb. 2014). *TINKER—Software tools for molecular design, Version 6.3, Copyright (C)*.
44. Andersen, H. C. (2008). Molecular dynamics simulations at constant pressure and/or temperature. *The Journal of Chemical Physics*, *72*, 2384–2393.
45. Barbatti, M., et al. (2022). Newton-X platform: New software developments for surface hopping and nuclear ensembles. *Journal of Chemical Theory and Computation*, *18*, 6851–6865.
46. Ostroumov, E., Müller, M. G., Marian, C. M., Kleinschmidt, M., & Holzwarth, A. R. (2009). Electronic coherence provides a direct proof for energy-level crossing in photoexcited lutein and  $\beta$ -carotene. *Physical Review Letters*, *103*, 108302.
47. Miki, T., et al. (2016). Vibronic coupling in the excited-states of carotenoids. *Physical Chemistry Chemical Physics*, *18*, 11443–11453.
48. Cupellini, L., Corbella, M., Mennucci, B., & Curutchet, C. (2018). Electronic energy transfer in biomacromolecules. *WIREs Computational Molecular Science*, *9*, 1.
49. Cignoni, E., Cupellini, L., & Mennucci, B. (2022). A fast method for electronic couplings in embedded multichromophoric systems. *Journal of Physics: Condensed Matter*, *34*, 304004.
50. Madjet, M., Abdurahman, A., & Renger, T. (2006). Intermolecular Coulomb couplings from ab initio electrostatic potentials: Application to optical transitions of strongly coupled pigments in photosynthetic antennae and reaction centers. *The Journal of Physical Chemistry B*, *110*, 17268–17281.
51. Frähmcke, J. S., & Walla, P. J. (2006). Coulombic couplings between pigments in the major light-harvesting complex LHC II calculated by the transition density cube method. *Chemical Physics Letters*, *430*, 397–403.
52. Gradinaru, C. C., van Stokkum, I. H., Pascal, A. A., van Grondelle, R., & van Amerongen, H. (2000). Identifying the pathways of energy transfer between carotenoids and chlorophylls in LHCII and CP29. A multicolor, femtosecond pump-probe study. *The Journal of Physical Chemistry B*, *104*, 9330–9342.
53. Fox, K. F., et al. (2017). The carotenoid pathway: What is important for excitation quenching in plant antenna complexes? *Physical Chemistry Chemical Physics*, *19*, 22957–22968.
54. Chmeliov, J., et al. (2015). An “all pigment” model of excitation quenching in LHCII. *Physical Chemistry Chemical Physics*, *17*, 15857–15867.
55. Holt, N. E., Kennis, J., Dall’Osto, L., Bassi, R., & Fleming, G. R. (2003). Carotenoid to chlorophyll energy transfer in light harvesting complex II from *Arabidopsis thaliana* probed by femtosecond fluorescence upconversion. *Chemical Physics Letters*, *379*, 305–313.